Chinese Journal of Integrative Medicine
Available online at link.springer.com/journal/11655
Journal homepage: www.cjim.cn/zxyjhen/zxyjhen/ch/index.aspx
E-mail: cjim_en@cjim.cn

Original Article

UPLC-Q-TOF/MS-Based Serum Metabolomics Reveals Potential Anti-tumor Mechanism of Banxia Xiexin Decoction in Colorectal Cancer Mice*

YUE Yin-zi[1], LI Ming-xuan[2], WANG Xiao-hui[3], QIN Yuan-yuan[4], WANG Ya-hui[5], TAN Jin-hua[3], SU Lian-lin[2], and YAN Shuai[5]

ABSTRACT **Objective**: To clarify the potential mechanism of Banxia Xiexin Decoction (BXD) on colorectal cancer (CRC) from the perspective of metabolomics. **Methods**: Forty male C57BL/6 mice were randomly divided into normal control (NC), azoxymethane/dextran sulfate sodium (AOM/DSS) model, low-dose BXD (L-BXD), high-dose BXD (H-BXD) and mesalamine (MS) groups according to a random number table, 8 mice in each group. Colorectal cancer model was induced by AOM/DSS. BXD was administered daily at doses of 3.915 (L-BXD) and 15.66 g/kg (H-BXD) by gavage for consecutive 21 days, and 100 mg/kg MS was used as positive control. Following the entire modeling cycle, colon length of mice was measured and quantity of colorectal tumors were counted. The spleen and thymus index were determined by calculating the spleen/thymus weight to body weight. Inflammatory cytokine and changes of serum metabolites were analyzed by enzyme-linked immunosorbent assay kits and ultra performance liquid chromatography-quadrupole/time-of-flight mass spectrometry (UPLC-Q/TOF-MS), respectively. **Results**: Notably, BXD supplementation protected against weight loss, mitigated tumor formation, and diminished histologic damage in mice treated with AOM/DSS ($P<0.05$ or $P<0.01$). Moreover, BXD suppressed expression of serum inflammatory enzymes, and improved the spleen and thymus index ($P<0.05$). Compared with the normal group, 102 kinds of differential metabolites were screened in the AOM/DSS group, including 48 potential biomarkers, involving 18 main metabolic pathways. Totally 18 potential biomarkers related to CRC were identified, and the anti-CRC mechanism of BXD was closely related to D-glutamine and D-glutamate metabolism, phenylalanine, tyrosine and tryptophan biosynthesis, arginine biosynthesis, nitrogen metabolism and so on. **Conclusion**: BXD exerts partial protective effects on AOM/DSS-induced CRC by reducing inflammation, protecting organism immunity ability, and regulating amino acid metabolism.

KEYWORDS colorectal cancer, metabolomics, ultra performance liquid chromatography-quadrupole/time-of-flight mass spectrometry, azoxymethane, dextran sulfate sodium, Banxia Xiexin Decoction, Chinese medicine

The occurrence and progression of colorectal cancer (CRC) are jointly caused by genetic modifications accumulated in cancer cells and surrounding microenvironment,[1] which is a complex process regulated by multiple periods and genes.[2] Currently, the pathogenesis of CRC is complex, and the treatment methods mainly consists of surgery, radiotherapy, and chemotherapy.[3] However, these treatments have a low cure rate and may cause irreversible damage to the body.[4,5] In terms of the macro level, CRC patients experience varying degrees of deterioration in body weight, tissues, organs, blood, urine, and feces. At the microscopic level, tumor cells have metabolic disorders, which have super proliferation and adversity survival abilities.[6] The occurrence and progression of CRC are closely related

*Supported by the Natural Science Foundation of Nanjing University of Chinese Medicine (No. XZR2020038); Science and Technology Innovation Project of Suzhou Medical and Health Care (No. SKJY2021136) and Fifth Batch of Gusu Health Personnel Training Project in Suzhou (No. GSWS2020085)
1. Department of General Surgery, Suzhou TCM Hospital Affiliated to Nanjing University of Chinese Medicine, Suzhou (215009), China; 2. School of Pharmacy, Nanjing University of Chinese Medicine, Nanjing (210023), China; 3. Department of General Surgery, Bayinguoleng Mongolian Autonomous Prefecture People's Hospital, Xinjiang Uygur Autonomous Region, Korla (841000), China; 4. Department of Pharmacy, Suzhou TCM Hospital Affiliated to Nanjing University of Chinese Medicine, Suzhou (215009), China; 5. Department of Anorectal Surgery, Suzhou TCM Hospital Affiliated to Nanjing University of Chinese Medicine, Suzhou (215009), China
Correspondence to: Prof. YAN Shuai, E-mail: doctor_shuaiyan@njucm.edu.cn
DOI: https://doi.org/10.1007/s11655-023-3552-0

to body's immune function and energy metabolism.[7] Some cytokines, such as interleukin (IL)-4, IL-10,[8] tumor necrosis factor (TNF)-α[9] and interferon (INF)-γ,[10] play an important role in the immune regulation of the body, and their expression levels are closely related to the occurrence and development of CRC. However, the above indicators cannot evaluate the occurrence and development of CRC disease and the effect of corresponding treatment methods comprehensively. Therefore, exploring the pathogenesis and treatment mechanism of CRC and finding accurate and effective biomarkers is very important.

Banxia Xiexin Decoction (半夏泻心汤, BXD) is derived from *Treatise on Febrile Diseases* (Wen Bing Lun). It is commonly used in the treatment of digestive system diseases in modern times.[11] Clinical study has shown that BXD has a good therapeutic effect on colon cancer and can significantly inhibit transition from colitis to colon cancer.[12] Literature research reveal the significant efficacy of BXD in aiding recovery of post-surgical CRC patients and preventing complications such as oral mucositis, nausea, vomiting, and delayed diarrhea in CRC patients undergoing chemotherapy.[13,14]

Metabolomics is a relatively recent field of systems biology. It focuses on small molecule metabolite alterations caused by environmental stressors or disruption.[15] It places a high value on the comprehensive examination of metabolites in an organism, which is consistent with holism philosophy of Chinese medicine (CM). Emerging metabolomics is being used to investigate the influence of CM on a variety of disorders.[16] Due to its high sensitivity, great reproducibility, and wide metabolome coverage, liquid chromatograph mass spectrometer, like nuclear magnetic resonance spectroscopy and gas chromatograohy-mass spectrometry, has gradually become one of the most high throughput technologies in metabolomic research and has gradually been used to evaluate the therapeutic effects of CM formula.[17-19]

Untargeted ultra performance liquid chromatography-quadrupole/time-of-flight mass spectrometry (UPLC-Q/TOF-MS)-based metabolomics were used in this study to evaluate the characteristics of the overall metabolic profile in sera of azoxymethane (AOM)/dextran sulfate sodium (DSS)-induced CRC mice and their pharmacological differences were compared. Metabolites produced in response to BXD treatment for CRC were discovered, and the underlying metabolic pathways were anticipated.

METHODS

Drugs, Reagents and Equipments

AOM and DSS were purchased from MP Biomedicals (lot No. 0216011080, 0218397125, USA). Mesalazine (MS) was purchased from Shanghai Aidefa Pharmaceutical Co., Ltd., China (Cat No. 210409). Recombinant human TNF-α (CSB-E04741m, lot No. P22039662), IFN-γ (CSB-E04578m, lot No. P22039663), IL-4 (CSB-E04634m, lot No. 005039664), and IL-10 (CSB-E04594m, lot No. 006039665) mouse enzyme linked immunosorbent assay (ELISA) kits were purchased from Cusabio Biotech Co., Ltd., China. Acetonitrile, methanol (chromatographically pure, Merck, Germany), Nexera UHPLC LC-30A (Shimadzu, Japan), MASS TripleTOF5600+, AB SCIEX™ (AB SCIEX, USA), tissue breaker (Bioprep-2, China) and Vortex instrument (XW-80A, China) were obtained.

BXD Preparation

Herbs of BXD (12 g *Pinellia ternata*, 3 g *Coptis chinensis*, 9 g *Scutellaria baicalensis*, 9 g *Rhizoma zngiberis*, 9 g *Radix ginseng*, 9 g *Roasted licorice* and 36 g *Fructus jujubae*) were provided from the Pharmacy Department of Suzhou TCM Hospital Affiliated to Nanjing University of Chinese Medicine and authenticated by Prof. LU Tu-lin, Nanjing University of Chinese Medicine. Based on the traditional decoction method, all herbs were firstly soaked in 10 times distilled waters of their total weight for 1 h, and then extracted by decoction two times. The final decoction was concentrated to required concentration (2.5 g/mL) using a rotary evaporator under reduced pressure to obtain a crude drug, sealed and stored at 4 ℃ for further use. Quality analysis of BXD extract was performed via high performance liquid chromatography (HPLC) fingerprinting.[20]

Animals

Forty male C57BL/6 mice (20.0±2.0 g, 8–10 weeks old) were purchased from Hunan Shrek Jingda Animal Experimental Co., Ltd., China [license No. SCXK(Xiang)2019-004]. All animals were housed under specific pathogen free condition at controlled temperature (25±2 ℃) and light (12 h light/dark cycle) with standard diet and water. The experimental procedures were approved by the Ethics Committee of Suzhou TCM Hospital Affiliated to Nanjing University

of Chinese Medicine (No. 2022LunDongPi054).

Grouping, Modeling and Treatment

All mice were randomly divided into 5 groups according to a random number table, 8 mice in each group, including normal control (NC), model (AOM/DSS), low-dose BXD (L-BXD), high-dose BXD (H-BXD) and MS groups. The experimental protocol was performed as described with few modifications.[21,22] The mice in the control group received distilled water, and the other 4 groups were given AOM/DSS to induce CRC. To establish the CRC model, each animal was intraperitoneally injected with 10 mg/kg of AOM dissolved in phosphate-buffered saline (PBS). One cycle consists of 7 days of 2.5% DSS followed by 14 days of regular water. Treatment began on day 42, and 2% DSS was also fed to the mice during the treatment process from day 42–63. From day 42, the mice in the L-BXD, H-BXD and MS groups were administrated with 3.915 g/kg BXD (1/2 times the amount of clinical use), 15.66 g/kg BXD (2 times the clinical dose for human) and MS (100 mg/kg, clinic equivalent dosage) by gavage, respectively, once a day, for consecutive 21 days, and the doses of BXD and MS were calculated from the human daily dose by using the body surface area normalization method. The mice in the NC and AOM/DSS groups received an equal volume of PBS.

Observation of Macroscopic Physical Signs

The body weight of all mice was recorded on days 0, 7, 14, 21, 28, 35, 42, 49, 56 and 63 during the process of modeling and administration, at the same time, the overall physiological states such as excretion of mice were observed and recorded. After 63 days of modeling and administration, all mice were sacrificed by cervical dislocation, and the colorectum was taken. The length of colon, size and number of tumors were measured, and state of abdominal organs were observed. The pathological samples were collected and fixed with paraformaldehyde (selected the colon with dense tumor distribution and folded the colon together from one side of the ileocecum), and part of the intestinal entrapment was randomly selected in the NC group.

Histopathological Observation of Colon and Spleen

The colon and spleen tissues fixed with 4% paraformaldehyde were routinely embedded in paraffin, serially cut into a thickness of 5 μm sections, and stained with hematoxylin-eosin (HE). The histopathological changes of the stained sections were observed under electron microscope.

Determination of Thymus and Spleen Index

Connective tissue was removed, and washed with 4 ℃ pre-cooled normal saline. After drying the surface moisture from the weight of the wet material, the thymus and spleen were weighed and the thymus and spleen index was calculated by comparing the thymus/spleen weight (g) to body weight (g).

Determination of TNF-α, IFN-γ, IL-4, and IL-10 Contents in Serum

The orbital blood of the mice was collected and placed at 4 ℃ for 2 h and centrifuged at 3,000 r/min for 15 min. The supernatant was prepared in the refrigerator at –20 ℃. The follow-up tests were carried out according to the instructions of TNF-α, IFN-γ, IL-4 and IL-10 ELISA kits.

Preparation of Biological Samples

Before the blood samples were collected, the mice were fasted for 12 h, and 1.5 mL blood was taken from the orbit to the blood vessels that contained anticoagulants after the modeling and administration on day 64, then the blood was shaken slowly for several times and centrifuged at 12,000 r/min, the supernatant was absorbed and stored at –80 ℃.

A serum sample (100 μL) was swirled with 400 μL solution (methanol: ceric ammonium nitrate = 1: 1, V/V) for 30 s and ultrasonic processed for 10 min (water bath, 4 ℃), incubated at –20 ℃ for 1 h to promote protein precipitation. After centrifuged at high speed and low temperature (13,000 r/min, 4 ℃) for 15 min, the supernatant was taken and evaporated to dry at 4 ℃ or room temperature with a vacuum concentrator. Then, 100 μL solution (acetonitrile: water= 1: 1, V/V) was added and swirled for 30 s, ultrasonic processed for 10 min (water bath, 4 ℃), centrifuged at 13,000 r/min and 4 ℃ for 15 min and the supernatant was detected.

Conditions of UPLC-Q-TOF/MS

Chromatographic Conditions

To obtain more comprehensive metabolic spectrum information, the following two chromatographic conditions were used for analysis. The analyte was separated on a Waters HSS T3 column (100 mm × 2.1 mm, 1.7 μm). The mobile phases were solvent A (0.1% formic acid

water) and solvent B (acetonitrile) with gradient elution (Appendix 1). The analyte was separated on a UPLC BEH Amide column (100 mm × 2.1 mm, 1.7 μm). The mobile phases were solvent A (0.1% formic acid water) and solvent B (acetonitrile) with gradient elution (Appendix 2). The analysis was carried out at a flow rate of 0.3 mL/min. The column temperature was set to 40 ℃. Totally 2 μL of sample was injected.

Mass Spectrometry Conditions

Mass spectrometry was performed on an LTQ-Orbitrap mass spectrometer connected to the UPLC instrument via ESI interface. Samples were analyzed in both negative and positive modes with the tune method set as follows: positive ion mode detection conditions: detection range: 60–1,000 m/z, ion source gas 1: 55 psi, ion source gas 2: 55 psi, air curtain gas: 35 psi, temperature: 550 ℃, DP: 80 V, CE: 10 V, ion spray voltage: 5,500 V. Negative ion mode detection conditions: detection range: 60–1,000 m/z, ion source gas 1: 55 psi, ion source gas 2: 55 psi, air curtain gas: 35 psi, temperature: 550 ℃. DP: –80 V, CE: –10 V, Ion spray voltage: –4,500 V.

Biomarker Identification and Construction of Metabolic Pathway

Biomarkers (differential metabolites) are endogenous small molecules that can objectively reflect physiological and pathological changes or external environmental stimuli in an organism, which generally have a molecular weight less than 1,000. To further clarify the differences in serum metabolites and find biomarkers with significant differences, independent samples *t*-test ($P<0.05$), variable importance in projection (VIP>1) and fold change (FC≥1.2) were combined to analyze the data between groups. The Human Metabolome Database (HMDB) and Kyoto Encyclopedia of Genes and Genomes (KEGG) database were also used for structure identification.

Data Analysis

All quantitative data are presented as the mean ± standard error of the mean (SEM) and were collected from at least 3 independent experiments. Differences between two groups were analyzed by an unpaired Student's *t* test using GraphPad Prism 9.0 (GraphPad, San Diego, CA, United States). One-way analysis of variance (ANOVA) was used for comparisons among more than two groups. Significance was recognized at a value of $P<0.05$. The UPLC-Q-TOF/MS spectrum and data were imported into the MarkerView software (SCIEX, USA) for peak extraction, matching and normalization pre-processing, and then pre-processed data was imported into the SIMCA-P14.1 software (Umetrics, Sweden) for orthogonal partial least-squares discriminant analysis (OPLS-DA) analysis. The differential metabolites were preliminarily obtained by statistical analysis of the data between groups. Then the chromatographic peaks of the differential metabolites were identified and matched by the PeakView software of Analyst® TF 1.6 software (SCIEX, USA) workstation, and the potential biomarkers were identified by standard chromatogram.

RESULTS

BXD Attenuated AOM/DSS-Induced Murine CRC

After the mice were induced by AOM/DSS, varying degrees of physiological discomfort were observed in vast majority of mice, such as mental malaise, diarrhea and severe hematochezia symptoms. The above symptoms were significantly ameliorated after administration of BXD and MS. As shown in Figure 1A, detailed body weight change during the entire experiment reflected the physiological status of the mice. Body weight loss was observed during each cycle of DSS administration in all groups of the mice that received AOM/DSS when compared with the NC group ($P<0.05$). BXD effectively alleviated DSS-induced weight loss. The effect of MS on the improvement of body weight in CRC mice was comparable to that of BXD ($P>0.05$). Meanwhile, treatment with BXD significantly increased the colon length, relative to the model group ($P<0.05$, Figures 1B–1C). Additionally, by analyzing the growth colon tumors, we observed that mice treated with H-BXD had decreased tumor incidence with notably lower average tumor load and less macroscopic tumors (number and size) than model group (Figures 1D and 1E).

HE Staining and Histological Scores

As shown in Figure 2, colon tissues of mice in the NC group consist of well-arranged mucosal epithelium, the basically intact colonic crypt glands and vacuolated cup-shaped cells. Compared with the NC group, the colonic mucosa of the model group was obviously damaged, crypt gland was atrophied, and its structure was disappeared or deformed locally, the structure of intestinal villi became thinner, goblet cells were nearly disappeared, and numerous inflammatory cell infiltration were appeared, which was consistent with

tumor tissue. After continuous administration of H-BXD and MS, the structural disruption and disturbance of the colonic crypt and colonic villi in mice were improved and massive infiltration of inflammatory cells was evidently ameliorated.

BXD Improved Inflammatory Level of CRC and Immune Function

As shown by the pathological section of spleen in Figure 3A, the white and red pulp of spleen in model group were increased, and blue lymphocytes were gathered in a region, which were decreased after H-BXD administration. As shown in Figure 3B, the spleen and thymus index of CRC mice were increased in varying degrees after BXD and MS administration, with the most significant growth in thymus index in the H-BXD group (P<0.01).

BXD Inhibited Serum Inflammation Cytokines Levels

Compared with the NC group, the levels of pro-inflammatory factors TNF-α, IFN-γ and IL-4 in the model group were increased remarkably (P<0.01), and the level of IL-10 decreased (P<0.05). In addition, the level of TNF-α in the H-BXD group was increased (P<0.01) and the levels of IL-4 and IFN-γ in H-BXD and MS groups were decreased significantly compared with model group (P<0.01, Figure 4).

Multivariate Analysis of Serum Metabolites

Based on the principal component analysis (PCA) results shown in Figures 5A and 5B, it was found that the degree of difference among all 5 groups was small, and the NC and model groups could be clearly distinguished from each other, indicating that significant differences

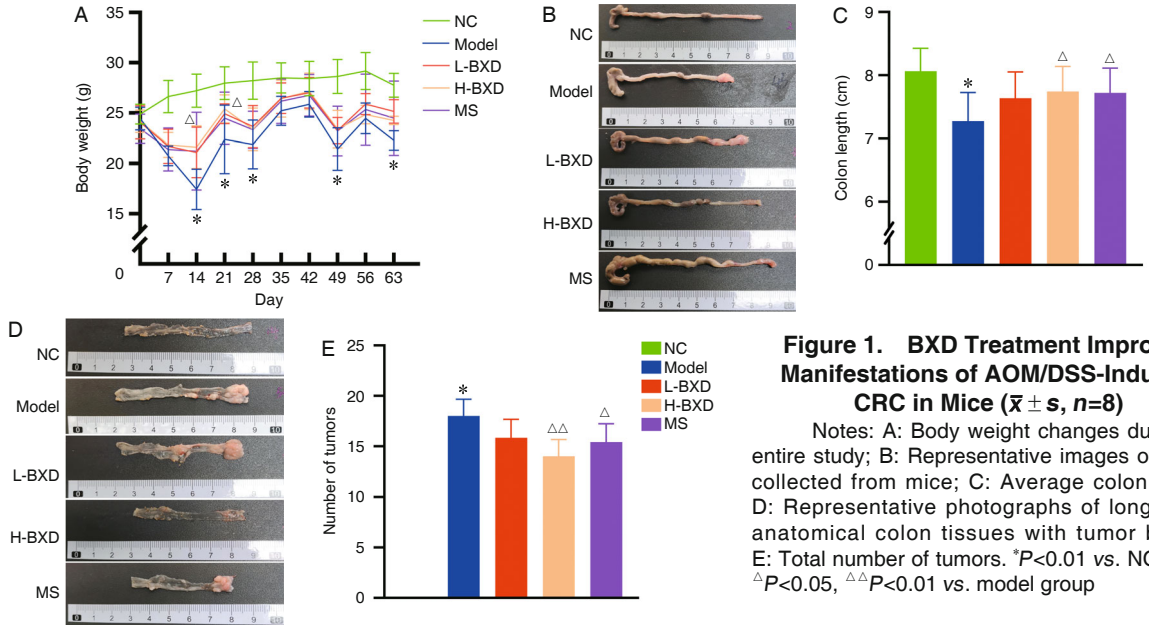

Figure 1. BXD Treatment Improves Manifestations of AOM/DSS-Induced CRC in Mice ($\bar{x} \pm s$, n=8)

Notes: A: Body weight changes during the entire study; B: Representative images of colons collected from mice; C: Average colon length; D: Representative photographs of longitudinal anatomical colon tissues with tumor burden; E: Total number of tumors. *P<0.01 *vs*. NC group; △P<0.05, △△P<0.01 *vs*. model group

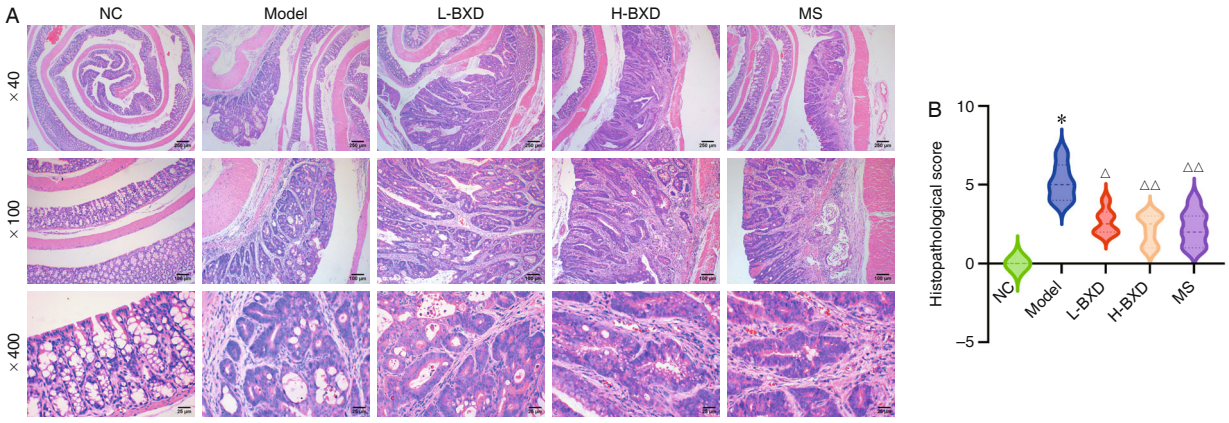

Figure 2. Histological Observations of Colon Tissues in Different Groups

Notes: A: Representative pathological images of colon (HE staining); B: Analysis of pathological scores ($\bar{x} \pm s$, n=8). *P<0.01 *vs*. NC group; △P<0.05, △△P<0.01 *vs*. model group

Chin J Integr Med 2024 Jul;30(7):623-632

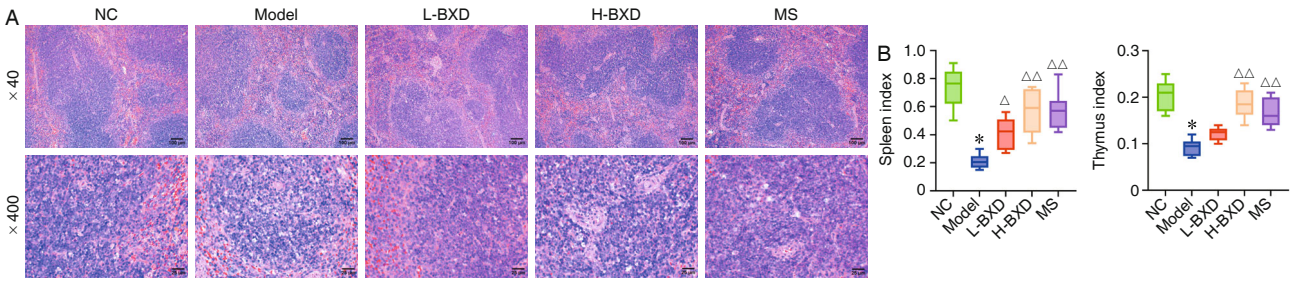

Figure 3. Regulatory Effect of BXD on Immune Organs in AOM/DSS-Induced CRC Mice

Notes: A: Representative pathological images of spleen; B: Spleen and thymus index changes of mice ($\bar{x} \pm s$, n=8). $^{*}P$<0.01 *vs*. NC group; $^{\triangle}P$<0.05, $^{\triangle\triangle}P$<0.01 *vs*. model group

were existed in serum endogenous metabolites between normal and CRC mice, and the successful modeling of CRC were further verified. Considering that PCA was a dimensionality reduction algorithm for unsupervised learning and did not visually reflect the differences between groups, the OPLS-DA analysis was used to highlight the differences among different groups.

As shown in Figure 5C, there were significant differences in serum metabolite distribution among the NC, model, L-BXD and H-BXD groups, which could achieve a better separation. Compared with the L-BXD group, the serum metabolic profile of the H-BXD group tended to the NC group, which preliminarily showed that BXD had a potential improvement effect on the serum metabolic disorder of CRC in mice, and the effect of the H-BXD was better. Based on the analysis in Figure 5E, it was also shown that the serum metabolic profile of MS group could also be significantly separated from NC and model groups, and its trend was similar to that of H-BXD, which further verified that BXD had potential regulatory effect on serum disorder in CRC mice. To verify the rationality and reliability of OPLS-DA model, 200 replacement experiments were carried out to test whether the two models were over-fitted. As shown in Figures 5D and 5F, the regression lines were linearly upward and the intercept between Q^2 and the Y-axis were negative, indicating that the two models were fit well, and the data could be described reliably and accurately.

Identification and Analysis of Differential Metabolites in Serum

The fitted parameters of the OPLS-DA models built for the NC *vs*. model and H-BXD *vs*. model groups were R^2X=0.669, R^2Y=1, Q^2=0.913 and R^2X=0.706, R^2Y=1, Q^2=0.747. It was indicated that both of above two OPLS-DA models were reliable, without over-fitting, and could be used to make predictions for differential metabolites.

As shown in Figure 6, 102 differential metabolites were identified in the comparison between NC and model groups, of which 47 metabolites were up-regulated and 55 metabolites were down-regulated. Totally 48 differential metabolites were identified between H-BXD and model groups. Among them, 31 metabolites were up-regulated, and 17 metabolites were down-regulated. Through the intersection of different metabolites obtained from 2 comparisons above (Appendix 3), it was found that BXD could pullback 18 kinds of metabolites, including pipecolic acid, hydroxyphenyl lactic acid, homocitrulline and alpha-keto isovaleric acid, etc. Eight of these were significantly pullback metabolites, including hydroxy isocaproic acid, hydroxyphenyl lactic acid, leucinic acid, 2-ethyl-2-hydroxybutyric acid, 2-hydroxycaproic acid, 3-hydroxymethylglutaric acid,

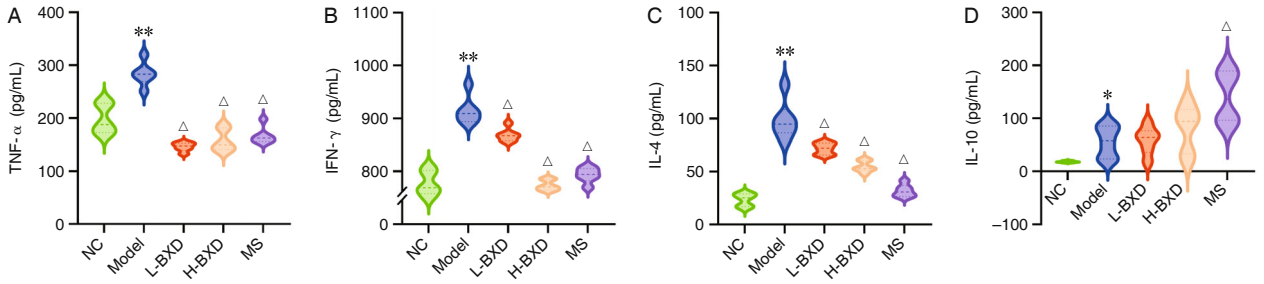

Figure 4. BXD Inhibited TNF-α, IFN-γ, IL-4 and IL-10 Expressions in Serum of AOM/DSS-Induced CRC Mice ($\bar{x} \pm s$, n=8)

Notes: $^{*}P$<0.05, $^{**}P$<0.01 *vs*. NC group; $^{\triangle}P$<0.01 *vs*. model group

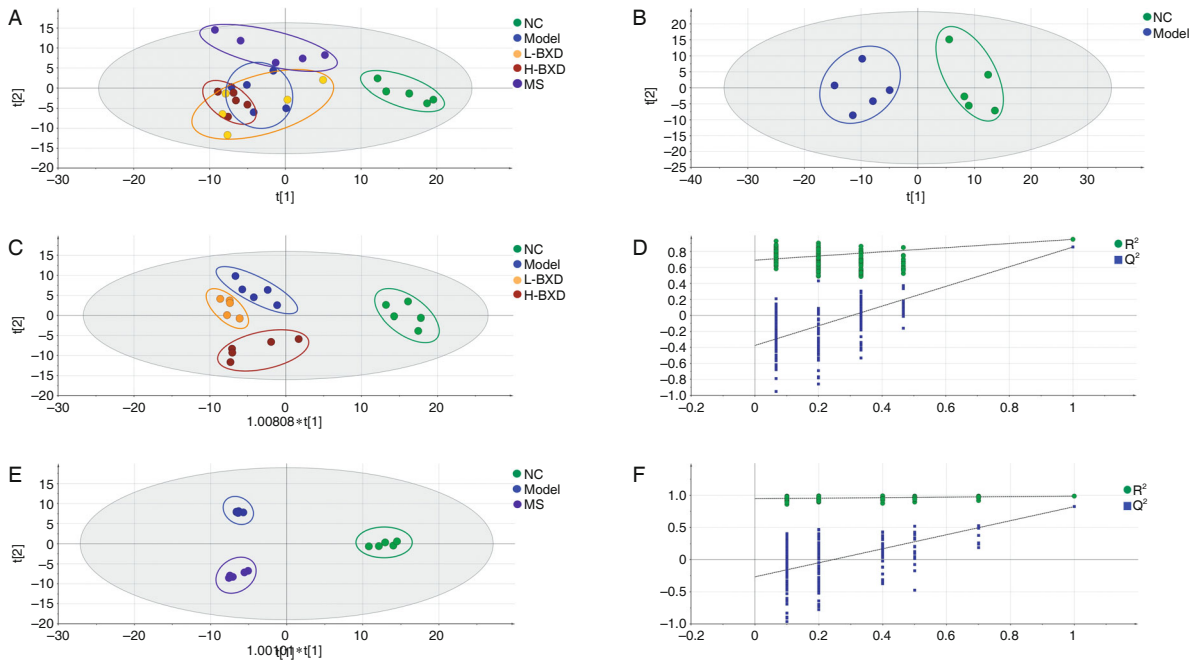

Figure 5. Multivariate Analysis Results of Serum Metabolites ($\bar{x} \pm s$, n=5)

Notes: A, B: PCA diagram of serum metabolites in mice. A: Whole groups; B: NC and model groups. C–F: OPLS-DA diagram of serum metabolites in mice. C, E: OPLS-DA score plot; D, F: 200 permutation test plots of the OPLS-DA model

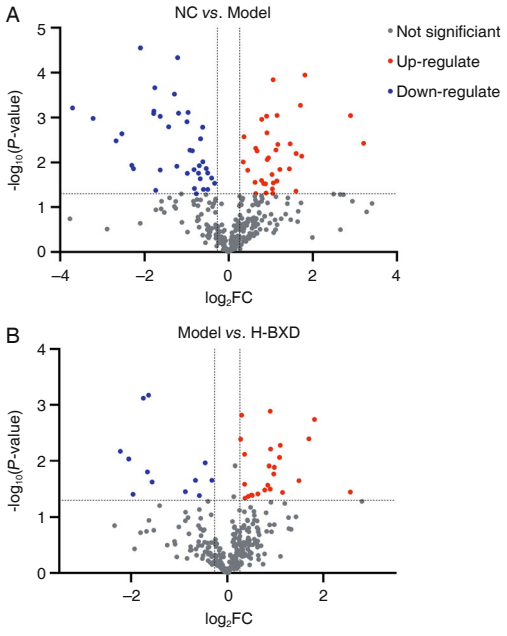

Figure 6. Volcano Plot of Differential Distribution of Serum Metabolites in Mice

Notes: Comparison between NC and model groups (A) as well as model and H-BXD groups(B). Red balls represent up-regulated metabolites; blue balls represent down-regulated metabolites. FC: fold change

pipecolic acid and malonic acid.

Metabolic Pathway Analysis of Differential Metabolites in Serum

As shown in Figure 7 and Appendix 4, the main metabolic pathways involved in the differential metabolites of serum samples in each group included arginine biosynthesis, phenylalanine, tyrosine and tryptophan biosynthesis, D-glutamine and D-glutamate metabolism, phenylalanine metabolism, nitrogen metabolism, alanine, aspartate, and glutamate metabolism, etc. It was clear that most of the metabolic pathways obtained by enrichment belong to amino acid synthesis and metabolism.

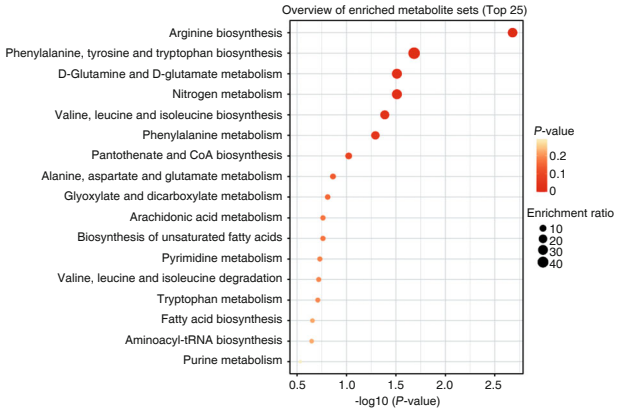

Figure 7. Metabolic Pathway Analysis Based on Potential Markers Identified in Serum Metabonomic

Note: The darker the color and the larger the area of the circle, the more important the metabolic pathway is

DISCUSSION

The treatment of intestinal diseases with BXD has been verified by numerous clinical and experimental

studies, however its mechanism remained unclear.[23,24] The multi-component and multi-target characteristics of CM also make it difficult to elucidate its effect mechanism directly.[25] From a microscopic point of view, metabolomics can more objectively and comprehensively clarify the mechanism of disease and the therapeutic effect of CM.

CRC is a malignant tumor of digestive system, patients have abnormal energy metabolism in their bodies, with a significant increase in metabolic rate and total consumption, and a significant decrease in the digestion, absorption, and utilization of nutrients. In recent years, the role of energy metabolism disorders in the development of CRC and the mechanisms involved gained more attention.[26] As the results of above study shown, the treatment of CRC with BXD was closely related to energy metabolism, mainly include the amino acid metabolism. During the growth of tumor cells, severe local tissue hypoxia and energy metabolism imbalance are caused by excessive tissue proliferation. The anaerobic degradation of glucose and aerobic respiration generate ATP, which is the main way to provide the energy source of the organism. Additionally, β-oxidation of fatty acids and the catabolism of amino acids and steroids to generate substrates for aerobic respiration of glucose can also generate copious amounts of ATP for the normal energy metabolism of the organism.[27] The occurrence and development of tumor is closely related to energy metabolism, and abnormal energy metabolism of tumor cells is an important feature that distinguishes tumor tissue from normal tissue. As structural and functional components of cells, amino acids are present in almost all types of cells. Free amino acids can be converted to produce organic acids through ammonia transfer, which are then catabolized to produce substrates for the tricarboxylic acid (TCA) cycle. As a source of energy, imbalances of amino acid metabolism in the body can also cause disturbances in energy metabolism.[28] Glutamine serves as the main form of nitrogen transport, it accounts for more than half of the total amino acids in the cycle. In addition, phenylalanine is mostly dependent on the conversion of tetrahydro pteridine to tyrosine.

Amino acid metabolism has been the focus of cancer research recently. When tumor cells proliferate rapidly and synthesize proteins, a large number of essential and non-essential amino acids are needed.[29] Glutamine is an important molecule in the metabolic regulatory network of CRC, it can be converted into α-ketoglutarate (α-KG) to enter TCA cycle (Krebs cycle) and acts as a key complementary component of TCA. Similarly, α-KG is also a raw material for the synthesis of nucleotides, fatty acids, and other non-essential amino acids.[30] Several enzymes and glutamine transporters involved in this process are regulated by miRNA.

Glutaminase 1 (GLS1) is an enzyme that catalyzes the formation of glutamate from glutamine. It has been noted that miR-137 can inhibit autologous stem cell transplantation (ASCT), in addition, the level of GLS1 can also be reduced. miR-137 was identified as a miRNA targeting GLS1, which is regulated by HSF1, it can be inhibited by heat shock transcription factor 1 (HSF1), because promoter methylation of the upstream gene mir137hg of miR-137 can reduce the expression of miR-137.[31] Therefore, the inhibition of GLS1 by miR-137 can hamper the decomposition and transformation of glutamine. Because glutamine is important for energy supply and molecular synthesis, miR-137 reduces the growth of CRC cells through this regulatory network. Glutamate is converted to α-ketoglutarate by glutamate pyruvate transaminase (GPT), which is a key component of TCA. CRC cells with the phosphatidylinositol-4,5-bisphospate 3-kinase catalytic subunit alpha isoform (PI3KCA) mutation have a higher requirement for glutamine due to the existence of catalytic subunit P110α. The increased expression of GPT2 are caused by this change in response to energy demands of rapid CRC growth and proliferation.[32] MiR-375 can bind to the PIK3CA-3'UTR and inhibits the expression of PIK3CA in CRC, thereby inhibits its growth through the PI3K/Akt pathway. The low expression of PI3K leads to the decrease in expression of GPT2, which limits the use of glutamine in CRC.

At present, the pathogenesis of CRC is unclear, limiting the provision of the best clinical treatment strategies and the most reasonable application of targeted drugs for patients. It is a commonly accepted view among researchers that energy metabolism in CRC patients is disturbed, and that the catabolism of 3 organic substances, sugars, lipids, and amino acids, is the main source of energy in living organisms.[30] Because of the complex pathogenesis of CRC, it is difficult to investigate the effects of a single substance

on the body. Metabonomic has special advantages in the study of the mechanism of complex diseases due to its high throughput, sensitivity, and accuracy. It can establish a direct correlation between the changes of metabolite content and biological phenotypic changes.[33-35] The use of metabolomics technology tools to study the mechanism of energy metabolism disorders in patients and find the metabolic pathways associated with the pathological state can provide a reference for the clinical diagnosis and treatment of CRC. Although we have examined the possible role of BXD in treating CRC, there are some limitations in the present study. We will further explore the dynamic changes in metabolites and validate BXD in the regulation of differential metabolomic in clinical patients.

Taken together, in the process of AOM/DSS-induced CRC, enteritis-relevant behavioral phenotype appeared, secretion levels of cytokine TNF-α, IFN-γ and IL-4 increased, immune function and energy metabolism disordered. This study identified potential biomarkers of CRC in mice, and established a correlation between them and BXD treatment. Future work might further identify the functional mechanisms by which metabolites are responsible for colorectal cancer conferred by BXD, and explore the applicability of BXD in CRC patients.

Conflict of Interest

The authors declare no conflicts of interest.

Author Contributions

Yue YZ, Yan S, Qin YY and Li MX designed the experiments. Wang XH, Qin YY and Wang YH performed experiments and collected the data. Tan JH and Su LL discussed the results and strategy. All authors read and approved the final version for publication.

Electronic Supplementary Material: Supplementary material (Appendixes 1–4) are available in the online version of this article at https://doi.org/10.1007/s11655-023-3552-0.

REFERENCES

1. Angell HK, Bruni D, Barrett JC, Herbst R, Galon J. The immunoscore: colon cancer and beyond. Clin Cancer Res 2020;26:332-339.
2. Luo XJ, Zhao Q, Liu J, Zheng JB, Qiu MZ, Ju HQ, et al. Novel genetic and epigenetic biomarkers of prognostic and predictive significance in stage Ⅱ/Ⅲ colorectal cancer. Mol Ther 2021;29:587-596.
3. Jain S, Maque J, Galoosian A, Osuna-Garcia A, May FP. Optimal strategies for colorectal cancer screening. Curr Treat Options Oncol 2022;23:474-493.
4. Biller LH, Schrag D. Diagnosis and treatment of metastatic colorectal cancer: a review. JAMA 2021;325:669-685.
5. Ramírez-Guerrero AA, González-Villaseñor CO, Leal-Ugarte E, Gutiérrez-Angulo M, Ramírez-Flores M, Delgado-Enciso I. Association between genetic variant rs2267716 of CRHR2 gene with colorectal cancer. J Investig Med 2022;70:947-952.
6. Henry CM. New 'ome' in town. Chem Eng News 2002;80:66-67.
7. Huo YR, Huang Y, Liauw W, Zhao J, Morris DL. Prognostic value of carcinoembryonic antigen (CEA), AFP, CA19-9 and CA125 for patients with colorectal cancer with peritoneal carcinomatosis treated by cytoreductive surgery and intraperitoneal chemotherapy. Anticancer Res 2016;36:1041-1049.
8. He J, Wang Z, Zhang S. Correlation analysis of IL-4, IL-10 and APN levels with postoperative infection of colorectal cancer. Oncol Lett 2019;17:1603-1608.
9. Banday MZ, Balkhi HM, Hamid Z, Sameer AS, Chowdri NA, Haq E. Tumor necrosis factor-α (TNF-α)-308G/A promoter polymorphism in colorectal cancer in ethnic Kashmiri population—a case control study in a detailed perspective. Meta Gene 2016;9:128-136.
10. Eissmann MF, Dijkstra C, Wouters MA, Baloyan D, Mouradov D, Nguyen PM, et al. Interleukin 33 signaling restrains sporadic colon cancer in an interferon-γ-dependent manner. Cancer Immunol Res 2018;6:409-421.
11. Ma L, Fang X, Yin X, Li Y. Investigation of molecular mechanism of Banxia Xiexin Decoction in colon cancer via network pharmacology and *in vivo* studies. Evid Based Complement Alternat Med 2022; 2022:4961407.
12. Yan S, Yue Y, Wang J, Li W, Sun M, Zeng L, et al. Banxia Xiexin Decoction, a traditional Chinese medicine, alleviates colon cancer in nude mice. Ann Transl Med 2019;7:375.
13. Nishikawa K, Aoyama T, Oba MS, Yoshikawa T, Matsuda C, Munemoto Y, et al. The clinical impact of Hangeshashinto(TJ-14) in the treatment of chemotherapy-induced oral mucositis in gastric cancer and colorectal cancer: analyses of pooled data from two phase Ⅱ randomized clinical trials (HANGESHA-G and HANGESHA-C). J Cancer 2018; 9:1725-1730.
14. Komatsu Y, Yuki S, Fuse N, Kato T, Miyagishima T, Kudo M, et al. Phase 1/2 clinical study of irinotecan and oral S-1(IRIS) in patients with advanced gastric cancer. Adv Ther 2010; 27:483-492.
15. Pinto RC. Chemometrics methods and strategies in metabolomics. Adv Exp Med Biol 2017;965:163-190.
16. Wang S, Wei S, Zhu Y, Zhang M, Cao X, Chang Y, et al.

Comparative investigation of the differences in chemical compounds between raw and processed *Mume Fructus* using plant metabolomics combined with chemometrics methods. Molecules 2022;27:6344.
17. Zhu B, Cao H, Sun L, Li B, Guo L, Duan J, et al. Metabolomics-based mechanisms exploration of Huang-Lian Jie-Du Decoction on cerebral ischemia via UPLC-Q-TOF/MS analysis on rat serum. J Ethnopharmacol 2018;216:147-156.
18. Pan B, Xia Y, Fang S, Ai J, Wang K, Zhang J, et al. Integrated network pharmacology and serum metabolomics approach deciphers the anti-colon cancer mechanisms of Huangqi Guizhi Wuwu Decoction. Front Pharmacol 2022;13:1043252.
19. Lu Q, Feng Q, Yu J, Tong L, Zhang J, Sun J, et al. Metabolomics and serum pharmacochemistry revealed the preventive mechanism of Gushudan in Kidney-yang-deficiency-syndrome rats. Biomed Chromatogr 2023;37:e5569.
20. Wang W, Gu W, He C, Zhang T, Shen Y, Pu Y. Bioactive components of Banxia Xiexin Decoction for the treatment of gastrointestinal diseases based on flavor-oriented analysis. J Ethnopharmacol 2022;291:115085.
21. Deng XQ, Zhang HB, Wang GF, Xu D, Zhang WY, Wang QS, et al. Colon-specific microspheres loaded with puerarin reduce tumorigenesis and metastasis in colitis-associated colorectal cancer. Int J Pharm 2019;570:118644.
22. Chartier LC, Fujino J, Howarth GS, Freysdottir J, Hardardottir I, Mashtoub S. Emu oil and Saireito in combination reduce tumour development and clinical indicators of disease in a mouse model of colitis-associated colorectal cancer. Biomed Pharmacother 2021;138:111478.
23. Zhang M, Huang W, Yuan D. Efficacy and safety of Banxia Xiexin Decoction as a complementary treatment for gastric cancer: a protocol for systematic review and meta-analysis. Medicine (Baltimore) 2021;100:e25747.
24. Yi Y, Hu Z, Li R, Chen L, Zhang H, Li H, et al. Effectiveness of Banxia Xiexin Decoction in the treatment of precancerous lesions: a protocol for systematic review and meta-analysis. Medicine (Baltimore) 2021;100:e25607.
25. Xiang Y, Guo Z, Zhu P, Chen J, Huang Y. Traditional Chinese medicine as a cancer treatment: modern perspectives of ancient but advanced science. Cancer Med 2019;8:1958-1975.
26. Schulze A, Schmidt C, Kohlmüller D, Hoffmann GF, Mayatepek E. Accurate measurement of free carnitine in dried blood spots by isotopedilution electrospray tandem mass spectrometry without butylation. Clin Chim Acta 2003;335:137-145.
27. Qiu Y, Cai G, Su M, Chen T, Zheng X, Xu Y, et al. Serum metabolite profiling of human colorectal cancer using GC-TOFMS and UPLC-QTOFMS. J Proteome Res 2009; 8:4844-4850.
28. Wijnen JP, van der Graaf M, Scheenen TW, Klomp DW, de Galan BE, Idema AJ, et al. *In vivo* ^{13}C magnetic resonance spectroscopy of a human brain tumor after application of ^{13}C-1 enriched glucose. Magn Reson Imag 2010; 28:690-697.
29. Van der Meij BS, Teleni L, Engelen MPKJ, Deutz NEP. Amino acid kinetics and the response to nutrition in patients with cancer. Int J Radiat Biol 2019;95:480-492.
30. Altman BJ, Stine ZE, Dang CV. From Krebs to clinic: glutamine metabolism to cancer therapy. Nat Rev Cancer 2016;16:619-634.
31. Miyagi Y, Higashiyama M, Gochi A, Akaike M, Ishikawa T, Miura T, et al. Plasma free amino acid profiling of five types of cancer patients and tis application for early detection. PLoS One 2011;6:e24143.
32. Wei XL, Liu FR, Liu JH, Zhao HY, Zhang Y, Wang ZQ, et al. First-in-human phase Ia study of the PI3Kα inhibitor CYH33 in patients with solid tumors. Nat Commun 2022;13:7012.
33. Chen F, Dai X, Zhou CC, Li KX, Zhang YJ, Lou XY, et al. Integrated analysis of the faecal metagenome and serum metabolome reveals the role of gut microbiome-associated metabolites in the detection of colorectal cancer and adenoma. Gut 2022;71:1315-1325.
34. Psychogios N, Hau DD, Peng J, Guo AC, Mandal R, Bouatra S, et al. The human serum metabolome. PLoS One 2013;8:e73076.
35. Heiles S. Advanced tandem mass spectrometry in metabolomics and lipidomics-methods and applications. Anal Bioanal Chem 2021;413:5927-5948.

(Accepted March 20, 2023; First Online May 24, 2023)
Edited by TIAN Lin